Role of dynamic pairing correlations in fission dynamics. II. Fermium and nobelium isotopes

R. Rodríguez-Guzmán[1,*] and L. M. Robledo[2,3,†]

[1]*Departamento de Física Aplicada I, Escuela Politécnica Superior, Universidad de Sevilla, Seville, E-41011, Spain*
[2]*Center for Computational Simulation, Universidad Politécnica de Madrid, Campus Montegancedo, 28660 Boadilla del Monte, Madrid, Spain*
[3]*Departamento de Física Teórica and CIAFF, Universidad Autónoma de Madrid, 28049-Madrid, Spain*

The competition between the quenching of pairing due to the repulsive Coulomb interaction and dynamic pairing correlations added by particle number symmetry restoration has been studied in a selected set of Fermium and Nobelium isotopes by using a hierarchy of Hartree-Fock-Bogoliubov–based approximations and a restricted variation after particle number projection, all of them based on the D1M* parametrization of the Gogny force. It is found that Coulomb antipairing is partially compensated by beyond-mean-field pairing correlations. However, the compensation is not perfect and a modulation of the spontaneous fission half-lives, as functions of the neutron number, indicates that the combined effect on fission dynamics of Coulomb antipairing and restricted particle number symmetry restoration cannot be overlooked. Neither can it be accounted for by the Coulomb Slater approximation.

I. INTRODUCTION

An accurate description of the evolution of the nuclear shapes from the ground state to scission still remains a main challenge for modern nuclear structure models of fission [1]. Within the mean-field framework, shape changes along the fission path are usually accounted for with the help of constrains [2] on some deformation parameters **Q** (see, for example, Refs. [1,3] and references therein).

In the case of *least-energy* approximations, each **Q**-deformed configuration along the fission path is obtained via the self-consistent Ritz-minimization [2] of the corresponding mean-field energy. The mean-field framework also provides collective inertias as well as quantum zero-point rotational and vibrational corrections [3], which are employed to compute spontaneous fission half-lives t_{SF} within the Wentzel-Kramers-Brillouin (WKB) framework. Microscopic mean-field calculations are typically carried out with nonrelativistic Gogny [4–13], Skyrme [14–18], and Barcelona-Catania-Paris-Madrid (BCPM) [19–21] or relativistic [22–28] energy density functionals (EDFs).

The fission properties of even-even Ra, U, Pu and selected superheavy isotopes have been studied in recent years within the framework of the least-energy approach using several parametrizations of the Gogny-EDF [3,29,30]. Fission studies have also been carried out for odd-mass U, Pu, and No nuclei [31,32] within the equal filling approximation (EFA) [33]. Special attention has been paid to the uncertainties in the predicted t_{SF} values. In particular, it has been found that modifications of a few percent in the pairing strengths can have a significant impact on the collective masses leading to uncertainties of several orders of magnitude in the lifetime values.

In the case of *least-action* approximations, each configuration along the fission path is obtained via the minimization of the collective action written in terms of a relevant set of deformation parameters. It has been shown [34,35] that the least energy and least action schemes only provide similar results when shape deformation degrees of freedom are used in the evaluation of the action. However, in the case of pairing degrees of freedom, it is known that the collective action depends on the competition between the collective inertia (decreasing as the inverse of the square of the pairing gap [36,37]) and the energy (increasing as the square of the pairing gap). This competition results in a minimum of the action located at a pairing gap larger than the one corresponding to the minimum-energy configuration. The value of the action at the minimum is substantially reduced as compared with the one obtained for the minimum-energy configuration. As shown in previous studies [34,35,38–43] the reduction of the action leads to a decrease of a few orders of magnitude in the computed t_{SF} values as compared with those obtained within the least energy approach. These effects clearly reflect the importance of pairing degrees of freedom in the description of fission dynamics.

The least energy and least action results already mentioned point towards the need to better understand the impact of pairing correlations in fission calculations. Dynamic pairing correlations, associated with fluctuations in the pairing's order parameter and/or symmetry restoration of the particle number symmetry, represent an important component of the pairing contents of a nuclear system and therefore they are expected to modify the conclusions extracted from a pure mean-field calculation regarding fission dynamics. In a previous study

*raynerrobertorodriguez@gmail.com
†luis.robledo@uam.es

[44], the impact of particle number symmetry restoration in spontaneous fission half-lives was analyzed in a couple of nuclei with rather high and wide fission barriers. The conclusion reached is that the different effects associated with the particle number projection (PNP) method somehow compensate and the impact on t_{SF} values is rather limited. In this paper we extend the previous study [44] to consider, within the same framework, a selected set of fermium and nobelium isotopes with much lower and narrower fission barriers. To this end, the restoration of the U(1) gauge (particle number) symmetry, spontaneously broken at the Hartree-Fock-Bogoliubov (HFB) level [2], via particle number projection is considered.

Unfortunately, the computational cost of beyond-mean-field methods prevents their systematic application to fission studies (see, for example, Refs. [44–48]). One of the reasons is that, in order to avoid the self-energy problem associated with the breaking of the Pauli principle [49,50], it is not allowed to neglect some of the direct, exchange or pairing contributions coming from some parts of the interaction. This is particularly cumbersome in the case of the Coulomb interaction, as the quenching of pairing correlations (Coulomb antipairing), usually neglected due to the computational effort associated with the evaluation of Coulomb's pairing field, have to be taken into account explicitly. Coulomb antipairing leads to a reduction of the pairing gap [51,52] and therefore collective inertias, with their inverse dependence on the square of the pairing gap, will increase when this contribution is included, leading to an increase of the collective action and longer spontaneous fission half-lives. On the other hand, dynamic pairing correlations tend to increase the pairing gap reducing thereby the collective inertias. It is the aim of this paper to study the systematic of those competing effects, i.e., Coulomb antipairing and dynamic pairing, in the set of nuclei $^{242-262}$Fm and $^{250-264}$No, for which experimental data are available [53]. The choice of these isotopic chains is not accidental, in a previous study [44] we carried out similar calculations in a couple of isotopes with rather high and wide fission barriers. One of the purposes of this paper is to confirm or dismiss the conclusions reached in Ref. [44] in the present case, with much lower and narrower fission barriers.

One has to keep in mind that the evolution of the nuclear shapes along the fission path affects the level density around the Fermi energy. This is associated with a complex pattern in the behavior of pairing correlations, including regions of very small and/or vanishing HFB pairing interaction energies [2]. To account for those effects, beyond-mean-field (i.e., dynamic) pairing correlations should be included within the PNP scheme. Moreover, in order to gain additional correlations, the intrinsic HFB wave functions have to be determined by minimizing the particle-number-projected energy, a procedure known as variation after PNP (VAP-PNP) [49].

In this paper, as in previous studies [44,54,55], we resort to a *restricted* VAP-PNP (RVAP-PNP) scheme, which has already been shown to be superior to other alternatives such as the Lipkin-Nogami method [2,54,55]. Within the RVAP-PNP scheme, a variational subspace is built by projecting onto good proton and neutron number intrinsic HFB states constrained in both the proton $\langle \Delta \hat{Z}^2 \rangle$ and neutron $\langle \Delta \hat{N}^2 \rangle$ number fluctuations separately, where $\langle \cdots \rangle$ represents an average value in

the corresponding HFB state. Each optimal **Q**-configuration along the fission path is then determined by the minimum of the PNP energy in this subspace.

The results discussed in this paper have been obtained with the parametrization D1M* [56], which represents a recent reparametrization of the Gogny-D1M [57] EDF. The parametrization D1M* is defined as to have a larger slope of the symmetry energy coefficient in nuclear matter than the one in D1M. However, all the other relevant combinations of parameters keep their values as to preserve most of the properties of the Gogny-D1M EDF. The convenience of D1M* has been established in a previous large-scale study [13] of the fission properties of 435 superheavy nuclei using this parametrization.

The paper is organized as follows: In Sec. II, we briefly outline the methodology employed in this study. In particular, in this section we outline a hierarchy of HFB approximations as well as the RVAP-PNP method employed to compute the fission paths and spontaneous fission half-lives for the considered nuclei. The results of our calculations are discussed in Sec. III. First, in Sec. III A, we illustrate our methodology in the case of ^{250}Fm. The systematic of the fission paths and lifetimes, obtained with each of the considered theoretical approaches, is discussed in Sec. III B for $^{242-262}$Fm and $^{250-264}$No. Finally, Sec. IV is devoted to the concluding remarks and work perspectives.

II. THEORETICAL FRAMEWORK

In the present study we use as a starting point the HFB approximation, with the D1M* parametrization [56] of the Gogny-EDF. Fission paths are obtained with the help of constrains on the mean value of the axially symmetric quadrupole $\hat{Q}_{20}$ and octupole $\hat{Q}_{30}$ operators [13,58,59]. Constrains on the proton $\Delta \hat{Z}^2$ and neutron $\Delta \hat{N}^2$ number fluctuation two-body operators [35,43,44] are included to implement the RVAP-PNP approach mentioned in the introduction. The new constraints require two additional terms in the Routhian

$$-\lambda_{\Delta \hat{Z}^2} \Delta \hat{Z}^2 - \lambda_{\Delta \hat{N}^2} \Delta \hat{N}^2, \qquad (1)$$

with the corresponding chemical potentials $\lambda_{\Delta \hat{Z}^2}$ and $\lambda_{\Delta \hat{N}^2}$. The minimization process is restricted to satisfy the conditions $\langle \Delta \hat{Z}^2 \rangle = f_Z$ and $\langle \Delta \hat{N}^2 \rangle = f_N$ in the mean value of proton and neutron number fluctuation, where f_Z and f_N are the required values. In the gradient method used in the minimization this restrictions are implemented by imposing the gradient of the Routhian to be orthogonal to the gradients of proton and neutron number fluctuations. Those two-body operator gradients are computed in analogy with the gradient of the energy. Although it will not be mentioned explicitly, in all the HFB calculations discussed below, aside from the usual constrains on both the proton and neutron numbers [2], a constrain on the operator $\hat{Q}_{10}$ is used to prevent spurious effects due to the center of mass motion [58,59]. Note, that parity is allowed to be broken at any stage of the calculation.

As it is customary in this kind of calculation, the HFB quasiparticle operators are expanded in an axially symmetric (deformed) harmonic oscillator (HO) basis containing states with J_z quantum numbers up to 35/2 and up to 26 quanta in
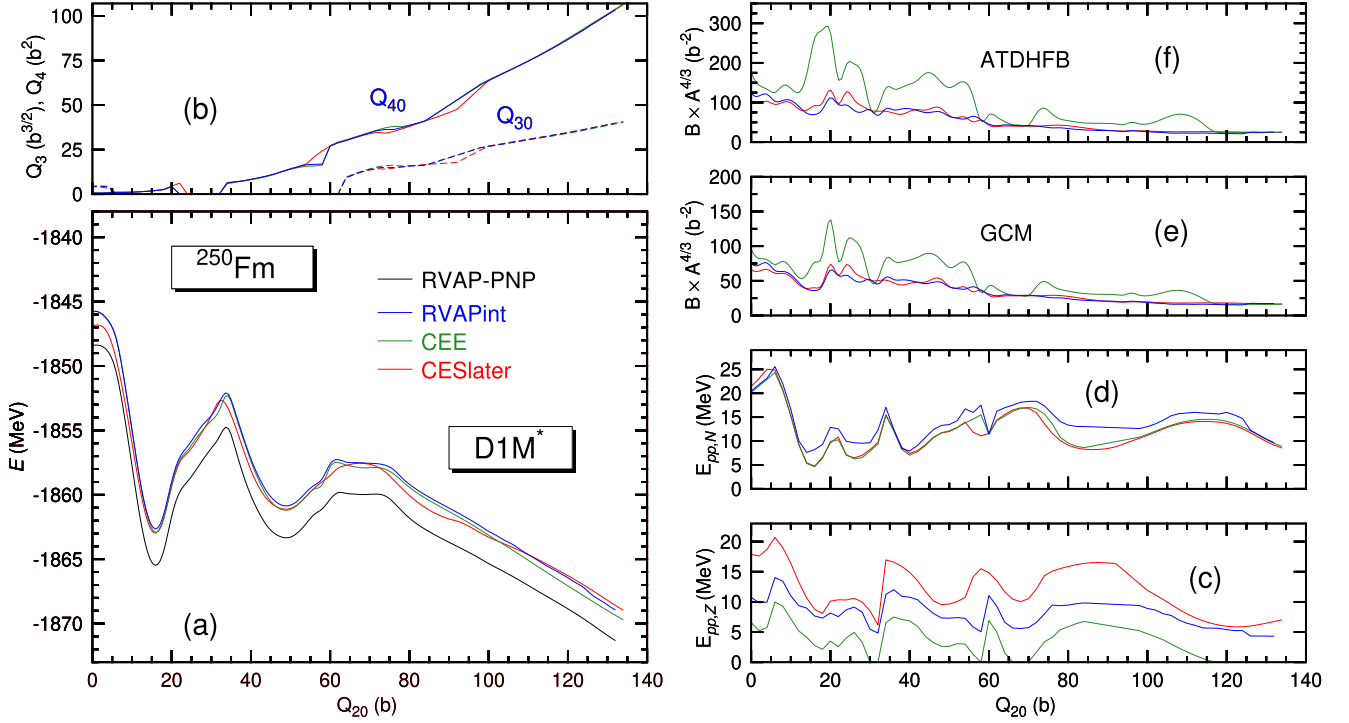
FIG. 1. The HFB(CESlater), HFB(CEE), HFB(RVAPint), and RVAP-PNP energies plus the zero-point rotational energies obtained for the nucleus ^{250}Fm are plotted in panel (a) as functions of the quadrupole moment Q_{20} of the intrinsic states. The octupole Q_{30} and hexadecapole Q_{40} moments corresponding to HFB(CESlater), HFB(CEE), and HFB(RVAPint) states are plotted in panel (b). The proton $E_{pp,Z}$ and neutron $E_{pp,N}$ pairing interaction energies corresponding to those intrinsic states are plotted in panels (c) and (d), while the collective GCM and ATDHFB masses are plotted in panels (e) and (f). Results have been obtained with the parametrization D1M* of the Gogny-EDF. For more details, see the main text.

the z direction. More specifically, the basis quantum numbers are restricted by the condition

$$2n_\perp + |m| + qn_z \leqslant M_{z,\text{MAX}}, \qquad (2)$$

with $M_{z,\text{MAX}} = 17$ and $q = 1.5$ [3,29,32]. For the solution of the HFB equations, an approximate second-order gradient method [60] has been used.

In the RVAP-PNP approach, for each specific value of the quadrupole and octupole moments, the HFB wave functions $|\Phi(f_Z, f_N)\rangle$ are used to compute the PNP projected energy,

$$E^{Z,N}(Q_{20}, Q_{30}, f_Z, f_N) = \frac{\langle\Phi|\hat{H}\hat{P}^Z\hat{P}^N|\Phi\rangle}{\langle\Phi|\hat{P}^Z\hat{P}^N|\Phi\rangle}, \qquad (3)$$

and the f_Z and f_N values of the intrinsic state are chosen as to minimize the projected energy. This is a kind of VAP-PNP but considering a restricted set of intrinsic states. In the above expression, $\hat{P}^Z$ and $\hat{P}^N$ are the standard particle number projector

$$\hat{P}^N = \frac{1}{2\pi} \int_0^{2\pi} d\varphi e^{i\varphi(\hat{N}-N)}.$$

In the evaluation of the PNP energy, the direct, exchange, and pairing channels for each of the terms of the Gogny-D1M* EDF have been computed to avoid the appearance of divergences connected with the self-energy problem and the violation of the Pauli principle [49,50]. The Hamiltonian and norm overlaps between intrinsic ($|\Phi\rangle$) and gauge-rotated

($e^{i\varphi\hat{N}}|\Phi\rangle$) states which are required for the calculation of the PNP energies are obtained using the generalized Wick theorem [61,62]. In the evaluation of the projected energy in Eq. (3), the PNP density prescription discussed in Refs. [44,49,50] has been used for the density-dependent part of the Gogny-D1M* EDF.

With these tools at hand, a series of calculations, as described below, are carried out to understand the role of the different ingredients considered in this work. To illustrate the practical aspects of the methodology used, we consider the nucleus ^{250}Fm, as a typical example. More specifically, we have carried out the following calculations:

Step 1. HFB(CESlater): We first obtained the (least energy) fission path for ^{250}Fm. To this end, we have resorted to the (Q_{20}, Q_{30})-constrained HFB approximation. The two length parameters b_z and $b_\perp$ characterizing the axially symmetric HO basis have been optimized for each (Q_{20}, Q_{30}) configuration [3,31]. In the calculations, Coulomb exchange is evaluated in the Slater approximation [63] while Coulomb and spin-orbit antipairing are neglected. Quantum zero-point rotational and vibrational energies have been added *a posteriori* to the HFB energy. The HFB(CESlater) plus rotational correction energy is plotted in Fig. 1(a) as a function of the quadrupole moment. The zero-point vibrational energy is not included in the plot,

as it is rather constant as a function of Q_{20}. However, such vibrational correction energy is always included in the computation of the corresponding t_{SF} values.

Step 2. HFB(CEE): Next, we determined the HFB(CEE) fission path for ^{250}Fm. To this end, we have performed (Q_{20}, Q_{30})-constrained HFB calculations in which both the contribution of the repulsive Coulomb interaction to the Hartree-Fock exchange potential and the pairing field[1] have been fully considered. The (optimized) HFB(CESlater) intrinsic wave functions (Step 1) have been used as starting input in the Ritz-variational procedure. No optimization of the HO lengths has been performed at this stage as the oscillator lengths are strongly connected to the deformation parameters of the configuration considered. Quantum zero-point rotational and vibrational energies have, once more, been added *a posteriori* to the HFB(CEE) energies. The HFB(CEE) plus rotational correction energy is plotted in Fig. 1(a).

Let us mention that in calculations where the proton and neutron pairing strengths are independently adjusted to experimental data in the region of interest [64], Coulomb antipairing is taken into account effectively by the fitted pairing strengths. However, for Gogny-like EDFs, the neutron pairing strength is fit to experimental data in tin isotopes, while the proton pairing strength comes from isospin invariance. As a result, Coulomb antipairing should be explicitly taken into account as to improve agreement with experimental proton pairing gaps.

Step 3. HFB(RVAPint) and RVAP-PNP: With the HFB(CEE) intrinsic states (Step 2) at hand, they are used as initial input in constrained calculations where, for each (Q_{20}, Q_{30}) configuration, intrinsic HFB wave functions have been generated constraining the proton $f_Z = \langle \Delta \hat{Z}^2 \rangle$ and neutron $f_N = \langle \Delta \hat{N}^2 \rangle$ number fluctuations, separately. The intrinsic states HFB(RVAPint), for each (Q_{20}, Q_{30}) configuration, are obtained by minimizing the particle-number-projected energy of Eq. (3) with respect to the particle number fluctuation variables f_Z and f_N using a simple two-dimensional gradient method. In this way we obtain two different energies, one corresponding to the HFB energy of the intrinsic state, denoted as HFB(RVAPint); the other, corresponding to the PNP projected energy for that intrinsic state, denoted the RVAP-PNP energy. Rotational and vibrational energies, computed with the intrinsic HFB(RVAPint) states, have been added *a posteriori* to the HFB(RVAPint) and RVAP-PNP energies. The HFB(RVAPint) and

RVAP-PNP plus rotational correction energies are shown in Fig. 1(a).

For each of the HFB(CESlater), HFB(CEE), HFB(RVAPint), and RVAP-PNP approaches we have computed the spontaneous fission half-lives t_{SF} (in seconds) using the WKB formalism

$$t_{SF} = 2.86 \times 10^{-21} \times (1 + e^{2S}), \quad (4)$$

where the action S along the (one-dimensional Q_{20}-projected) fission path reads

$$S = \int_a^b dQ_{20} S(Q_{20}), \quad (5)$$

where the integrand $S(Q_{20})$ is defined as

$$S(Q_{20}) = \sqrt{2B(Q_{20})[V(Q_{20}) - (E_{min} + E_0)]}. \quad (6)$$

The integration limits a and b in Eq. (5) correspond to the classical turning points [36] of the potential-energy surface evaluated for the energy $E_{min} + E_0$. The energy E_{min} corresponds to the absolute minimum of the considered path, while E_0 accounts for the true ground-state energy once quadrupole fluctuations are taken into account. In this study, we have considered the commonly employed value 1.0 MeV for this parameter [3,30].

From its definition (4), it is evident that t_{SF} depends on the different approximations by means of the different potential-energy surfaces and collective inertias. The potential energy $V(Q_{20})$ in Eq. (6) is given by each of the HFB(CESlater), HFB(CEE), HFB(RVAPint), and RVAP-PNP energies corrected by the zero-point vibrational and rotational energies. In the case of intrinsic HFB(CESlater), HFB(CEE), HFB(RVAPint) states, the collective mass $B(Q_{20})$ as well as the zero-point vibrational energy correction are computed using two methods. One is the perturbative cranking approximation [65–67] to the adiabatic time-dependent HFB (ATDHFB) scheme. The second method is based on the Gaussian overlap approximation (GOA) to the GCM [2]. On the other hand, the rotational energy correction has been computed in terms of the Yoccoz moment of inertia [68–70]. Due to the lack of an appropriate theoretical framework in the RVAP-PNP case, we have pragmatically employed the collective masses as well as the zero-point rotational and vibrational energies obtained with the HFB(RVAPint) intrinsic states [44].

III. DISCUSSION OF THE RESULTS

In this section, the results of our calculations are discussed. First, to set the stage, the methodology employed to compute the fission paths and other fission-related quantities in the case of ^{250}Fm are discussed in Sec. III A as an illustrative example. In Sec. III B the same methodology is systematically employed for all the studied nuclei $^{242-262}$Fm and $^{250-264}$No.

A. An illustrative example: The nucleus ^{250}Fm

The HFB(CESlater), HFB(CEE), HFB(RVAPint), and RVAP-PNP plus zero-point rotational energies are plotted for

---

[1]This contribution is usually called Coulomb antipairing due to the repulsive character of the Coulomb interaction, which reduces the pairing gap of protons.
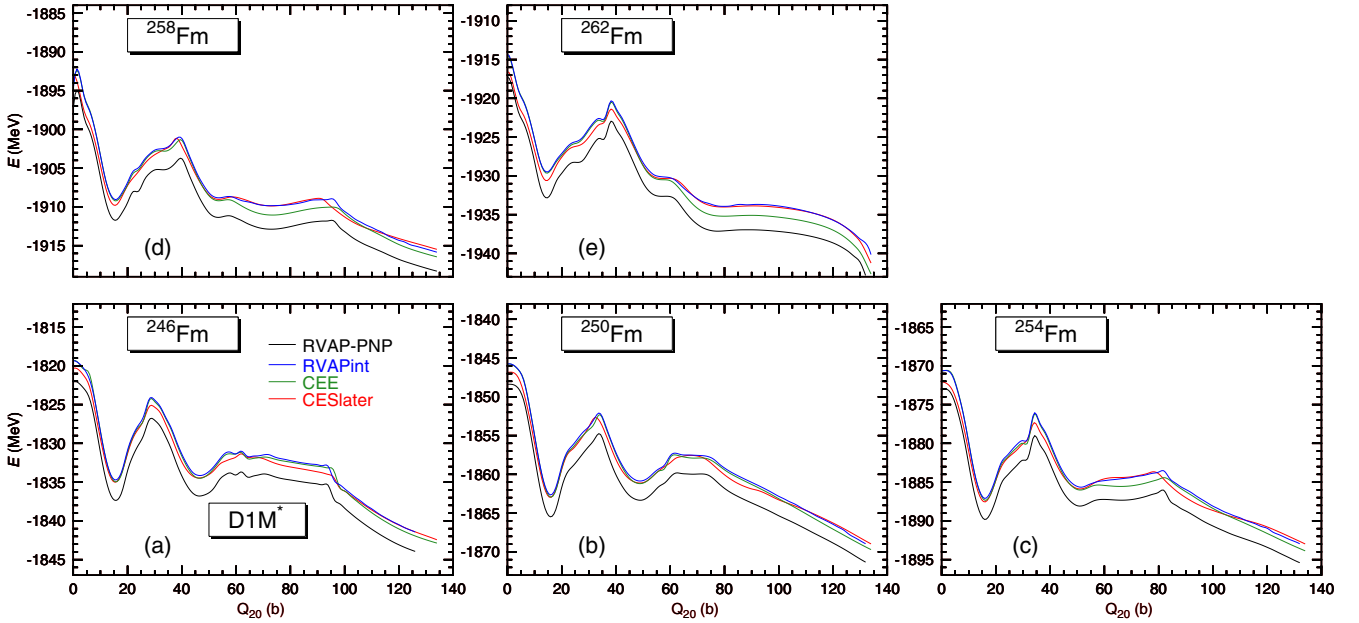
FIG. 2. The HFB(CESlater), HFB(CEE), HFB(RVAPint), and RVAP-PNP energies plus the zero point rotational energies obtained for the nuclei ^{246,250,254,258,262}Fm are plotted in panels (a) to (e) as functions of the quadrupole moment Q_{20} of the intrinsic states. Results have been obtained with the parametrization D1M* of the Gogny-EDF.

the nucleus ^{250}Fm in Fig. 1(a) as functions of the quadrupole moment Q_{20} of the intrinsic states. The reflection symmetric ($Q_{30} = 0$) absolute minimum of each path is located at $Q_{20} = 16$ b. The fission isomer at $Q_{20} = 48$ b is separated from the ground state by the inner barrier, the top of which is located at $Q_{20} = 32$–34 b. As in the ground-state case, the fission isomer is reflection symmetric. Octupole correlations play a prominent role for quadrupole deformations $Q_{20} \geqslant 62$ b. Those correlations significantly affect the height of the outer barrier, the top of which is located at $Q_{20} = 68$ b in the HFB(CESlater) case. A second barrier with more structure and with the top located at $Q_{20} = 62$ b is obtained within the HFB(CEE), HFB(RVAPint) and RVAP-PNP approaches. For large quadrupole moments ($Q_{20} \geqslant 100$ b) the HFB(CEE) and HFB(RVAPint) paths exhibit a faster decline than the HFB(CESlater) path. The RVAP-PNP path is around 2.5–3.0 MeV deeper than the others.

We have obtained the HFB(CESlater), HFB(CEE), HFB(RVAPint), and RVAP-PNP values 10.25, 10.66, 10.55, and 10.72 MeV for the height B_I of the inner barrier, while for the excitation energy of the fission isomer we have obtained 1.88, 1.77, 1.82, and 2.17 MeV, respectively. For the height B_{II} of the outer barrier those approaches provide the values 5.41, 5.44, 5.38, and 5.64 MeV. The octupole Q_{30} and hexadecapole Q_{40} moments of the intrinsic states, plotted in Fig. 1(b), are rather similar in all the approximations.

The proton and neutron pairing interaction energies [2] $E_{pp,\tau} = \frac{1}{2}\mathrm{Tr}(\Delta_\tau \kappa_\tau)$ (with $\tau = Z, N$) of the intrinsic states are plotted in Figs. 1(c) and 1(d). Note that these quantities are meaningless in the RVAP-PNP case. As can be seen from Fig. 1(c), Coulomb antipairing severely quenches the proton pairing energies in the HFB(CEE) states as compared with the corresponding HFB(CESlater) values. However, the RVAP-PNP method softens this quenching of the proton

pairing energies as can be observed in the results for the HFB(RVAPint) intrinsic state. As can be seen from Fig. 1(d), the HFB(CESlater) and HFB(CEE) neutron pairing energies are, as expected, rather similar. On the other hand, larger $E_{pp,N}$ energies are obtained at the HFB(RVAPint) level.

The collective GCM and ATDHFB masses, computed in the perturbative cranking approximation [65–67] for the intrinsic states, are plotted in Figs. 1(e) and 1(f). A three-point filter has been employed to soften the wiggles in the masses [3]. Both kinds of masses display a similar trend but the ATDHFB masses are, on the average, larger than the GCM masses. Such differences can lead to differences of several orders of magnitude in the predicted spontaneous fission half-lives [3,29–32]. This is the reason to consider both the GCM and ATDHFB collective inertias in the computation of the t_{SF} values. Regardless of the considered GCM and/or ATDHFB scheme, the HFB(CEE) collective inertia is larger than the HFB(CESlater) inertia and exhibits pronounced high peaks. This is a consequence of the quenched proton pairing correlations in the former as compared with the latter [see Fig. 1(c)]. Nevertheless, the increased pairing correlations in the HFB(RVAPint) states lead to GCM and ATDHFB collective masses close to the corresponding HFB(CESlater) values.

The spontaneous fission half-lives are computed using Eq. (4) with both the GCM and ATDHFB inertias. For $E_0 = 1.0$ MeV, the values obtained with the HFB(CESlater), HFB(CEE), HFB(RVAPint), and RVAP-PNP approaches are $\log_{10} t_{\mathrm{SF}}^{GCM} = 9.88$, 15.22, 10.81, and 11.84 and $\log_{10} t_{\mathrm{SF}}^{\mathrm{ATDHFB}} = 12.53$, 21.71, 14.43, and 15.66, respectively. It is observed that the $t_{\mathrm{SF}}^{\mathrm{ATDHFB}}$ values are larger than the t_{SF}^{GCM} due to the systematic differences in the collective inertias obtained in each approach. In both the GCM and ATDHFB schemes the increase observed in the HFB(CEE) collective inertias, due to Coulomb antipairing, leads to a pronounced
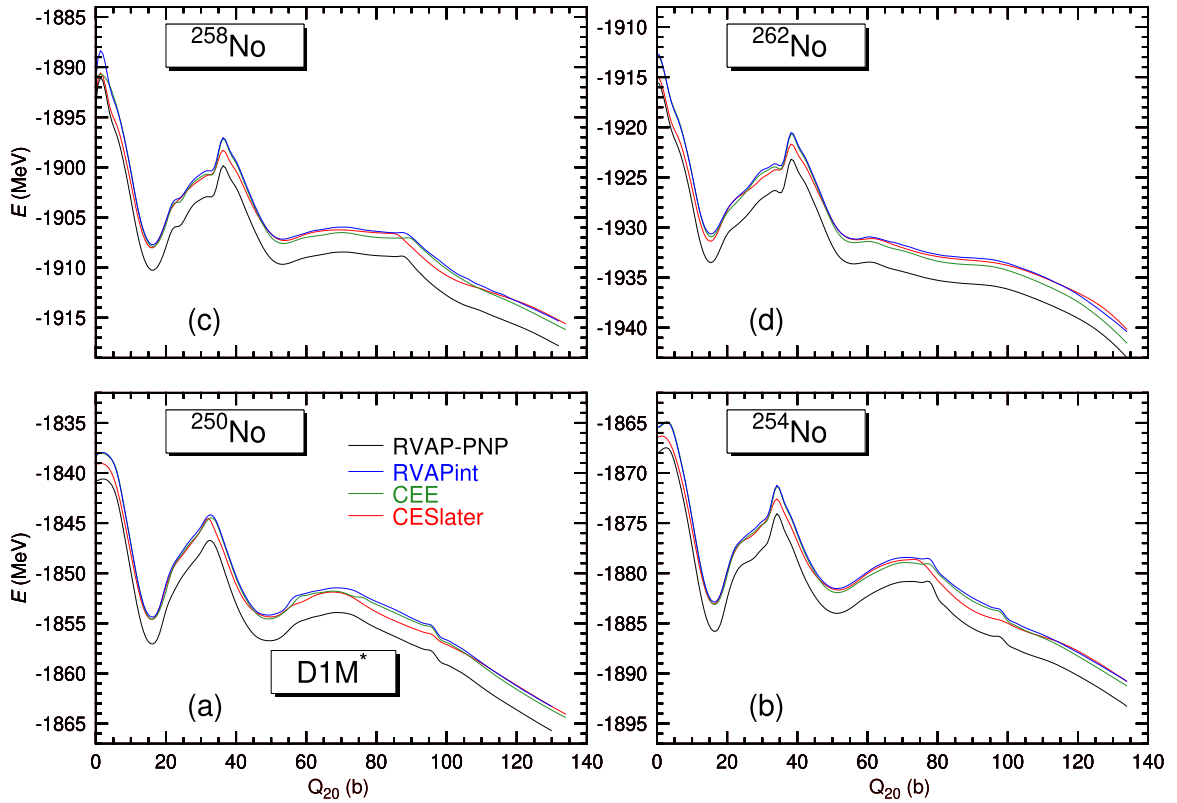
FIG. 3. The HFB(CESlater), HFB(CEE), HFB(RVAPint), and RVAP-PNP energies plus the zero point rotational energies obtained for the nuclei ^{250,254,258,262}No are plotted in panels (a) to (d) as functions of the quadrupole moment Q_{20} of the intrinsic states. Results have been obtained with the parametrization D1M* of the Gogny-EDF.

increase in the spontaneous fission half-lives. However, this huge increase is, to a large extent, canceled out by dynamic pairing correlations coming from particle number restoration. As a consequence, the HFB(RVAPint) and RVAP-PNP lifetimes get closer to the HFB(CESlater) values.

The results discussed in this section illustrate the competition between Coulomb antipairing and dynamic pairing effects in ^{250}Fm. Such a competition has also been found for a selected set of nuclei with wide fission paths, in a previous study [44]. It is therefore interesting to examine the impact of those competing effects on the systematic of the spontaneous fission half-lives and other fission related quantities along isotopic chains with lower barrier heights. This analysis is presented in the next section for the nuclei $^{242–262}$Fm and $^{250–264}$No. In the isotopic chains considered we find examples with wide fission paths as well as other cases where the corresponding fission paths display a faster decline in their more elongated sections.

B. Systematic of fission paths and spontaneous fission half-lives in $^{242–262}$Fm and $^{250–260}$No

In Figs. 2 and 3 we have plotted the HFB(CESlater), HFB(CEE), HFB(RVAPint), and RVAP-PNP energies plus the zero-point rotational energies obtained for the nuclei ^{246,250,254,258,262}Fm and ^{250,254,258,262}No, as functions of the quadrupole moment Q_{20} of the intrinsic state. A similar pattern is exhibited by other Fm and No nuclei and due to this,

they are not shown in the figures. For all of the studied nuclei, the RVAP-PNP path is around 2.0–3.5 MeV deeper than the others and the absolute minima of all the fission paths correspond to $Q_{20} = 12–16$ b.

In Fig. 4 we have plotted the proton $E_{pp,Z,GS}$ and neutron $E_{pp,N,GS}$ pairing interaction energies, as functions of the neutron number N, for the intrinsic ground states in $^{242–262}$Fm and $^{250–264}$No (these quantities are meaningless in the RVAP-PNP case). From Figs. 4(a) and 4(c), one realizes that Coulomb antipairing leads to a severe reduction of the HFB(CEE) $E_{pp,Z,GS}$ energies in comparison with the proton pairing energies obtained neglecting Coulomb antipairing. For example, the reduction amounts to 5.85, 6.00, 6.68, 7.44, and 8.27 MeV (5.63, 5.48, 5.98, and 6.83 MeV) in ^{246,250,254,258,262}Fm (^{250,254,258,262}No). Such a reduction is to a large extent canceled out, via RVAP-PNP, by dynamic pairing correlations. For example, we have found the energy differences $\Delta E_{pp,Z,GS}$ between the HFB(CESlater) and HFB(RVAPint) proton pairing energies to be 1.08, 1.11, 1.83, 2.63, and 4.16 MeV (1.09, 1.12, 1.98, and 2.57 MeV) for the nuclei already mentioned. On the other hand, as can be seen from Figs. 4(b) and 4(d) the neutron pairing energies in the HFB(RVAPint) ground states are larger than in the other mean-field approaches not incorporating dynamic pairing correlations. This illustrates the competition between Coulomb antipairing and dynamic pairing effects along the fission paths of the studied nuclei.

In Figs. 2 and 3, one notices that the maxima of the inner barriers are located in the interval $Q_{20} = 28–38$ b. The
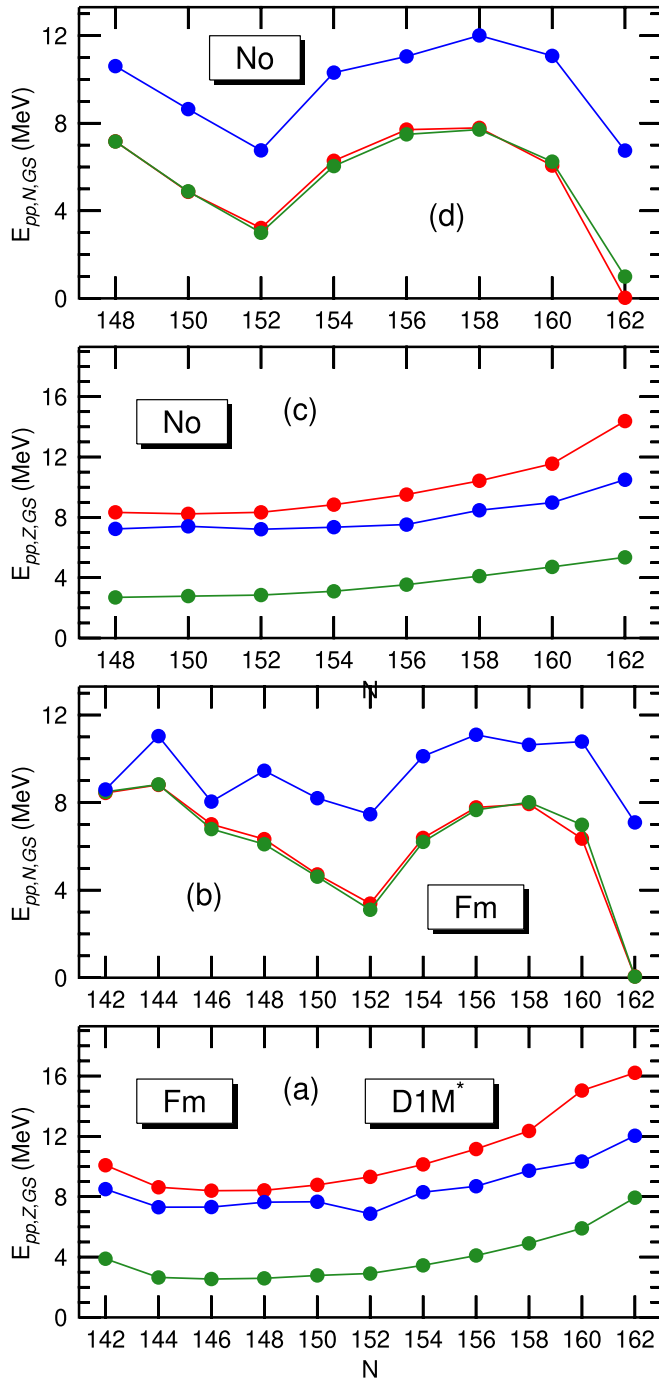
FIG. 4. The HFB(CESlater) (red), HFB(CEE) (green), and HFB(RVAPint) (blue) proton $E_{pp,Z,GS}$ and neutron $E_{pp,N,GS}$ ground-state pairing interaction energies obtained for $^{242-262}$Fm and $^{250-264}$No are plotted as functions of the neutron number N. Results have been obtained with the parametrization D1M* of the Gogny-EDF.

FIG. 5. The HFB(CESlater) (red), HFB(CEE) (green), HFB(RVAPint) (blue), and RVAP-PNP (black) inner barrier heights B_I obtained for $^{242-262}$Fm and $^{250-264}$No are plotted as functions of the neutron number N. Results have been obtained with the parametrization D1M* of the Gogny-EDF.

corresponding heights are plotted in Fig. 5 as functions of the neutron number N. Regardless of the employed approximation, the height B_I increases up to a maximum value in ^{252}Fm (^{254}No) and decreases for larger neutron numbers. For Fm isotopes [Fig. 5(a)], the HFB(CEE), HFB(RVAPint), and RVAP-PNP barrier heights are larger than the HFB(CESlater)

ones up to $N = 156$. For larger neutron numbers the situation is reversed, with larger HFB(CESlater) B_I values. On the other hand, for the considered No isotopes [Fig. 5(b)] the HFB(CEE), HFB(RVAPint), and RVAP-PNP barrier heights are always larger than the HFB(CESlater) values. The barriers heights B_I displayed in Fig. 5 have been obtained keeping axial symmetry as a self-consistent symmetry. Previous studies have shown that triaxial solutions can reduce the barrier heights by a few MeV (see, for example, Refs. [3,5,22]). However, it has also been found [18,26] that the lowering of the inner barrier comes together with an increase in the collective inertia that tends to compensate, in the calculation of the action, the reduction due to the lower triaxial barrier height. This result suggests that the axially symmetric path would be the preferred one in fission dynamics. Moreover, it has also been shown, that pairing fluctuations can restore axial symmetry along the fission path [41,71]. Therefore, the impact of triaxiality in the spontaneous fission half-lives seems to be very limited and it has not been considered in this study. If the triaxial degree of freedom were relevant, it would lead to a reduction of the spontaneous fission lifetime, and therefore
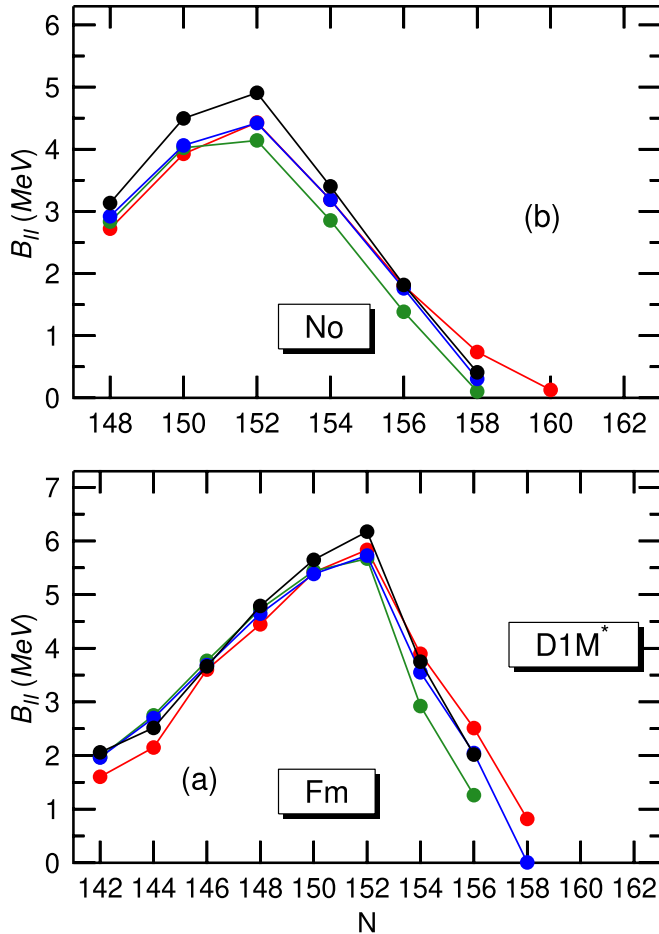
FIG. 6. The HFB(CESlater) (red), HFB(CEE) (green), HFB(RVAPint) (blue) and RVAP-PNP (black) outer barrier heights B_{II} obtained for $^{242-262}$Fm and $^{250-264}$No are plotted as functions of the neutron number N. Results have been obtained with the parametrization D1M* of the Gogny-EDF.

the results presented in the present study should be considered as upper limits.

The large quadrupole sections of the fission paths shown in Figs. 2 and 3 also display fission isomers, located around $Q_{20} = 50$ b, as well as second barriers. The fission isomers are less pronounced in heavier isotopes as the outer barriers progressively disappear with increasing neutron number. The heights B_{II} of the second barriers are plotted in Fig. 6 as functions of the neutron number. For both Fm and No isotopes, regardless of the employed approximation, the height B_{II} reaches a peak at the neutron number $N = 152$ and decreases for larger neutron numbers. For Fm isotopes [Fig. 6(a)], the HFB(CEE), HFB(RVAPint), and RVAP-PNP barrier heights B_{II} are smaller than the HFB(CESlater) ones for $N \geqslant 154$, being the HFB(CEE) heights the smallest. The HFB(CEE) outer barrier disappears at $N = 156$ while it disappears at $N = 158$ in the other cases. For No isotopes [Fig. 6(b)], the HFB(CEE) barrier heights B_{II} are the smallest for $N \geqslant 152$. In this case, the HFB(CEE), HFB(RVAPint), and RVAP-PNP second barriers disappear at $N = 158$ while the HFB(CESlater) one disappears at $N = 160$.

We have computed the spontaneous fission half-lives Eq. (4) for the considered Fm and No isotopes. The HFB(CESlater), HFB(CEE), HFB(RVAPint), and RVAP-PNP spontaneous fission half-lives, predicted within the GCM [Fig. 6(a)] and ATDHFB [Fig. 6(b)] schemes, are depicted as functions of the neutron number in Figs. 7 and 8. Calculations have been carried out with a zero point energy $E_0 = 1.0$ MeV. One notices that the ATDHFB lifetimes are always larger than the GCM ones. For example, for ^{252}No we have obtained the HFB(CESlater), HFB(CEE), HFB(RVAPint), and RVAP-PNP values $\log_{10} t_{SF}^{GCM} = 5.15, 12.05, 6.68$, and 7.68, while $\log_{10} t_{SF}^{ATDHFB} = 6.78, 15.16, 9.19$, and 10.50. Increasing the value of E_0 (taken here as a free parameter) always leads to smaller t_{SF} values. Let us mention, that calculations have also been carried out with a zero-point energy E_0 estimated in terms of the curvature K of the fission path around the ground state and the ground-state collective quadrupole inertia M as $E_0 = \frac{1}{2}\sqrt{K/M}$. In all cases, we have found that the trend observed in the spontaneous fission half-lives, as functions of the neutron number N, is robust and qualitatively independent of the employed E_0 value. The trend in t_{SF} with neutron number closely follows the one obtained for the barrier heights in Figs. 5 and 6. Note, however, that the transmission probability through the fission barrier depends on several other ingredients, such as the barrier shape (mostly its width) and the behavior and size of the collective inertia, and is not solely determined by the barrier height as it is commonly argued.

It is also important to note that the impact of Coulomb antipairing gets approximately canceled out by the dynamic pairing correlations, induced via the RVAP-PNP procedure. One might get the wrong impression that the results obtained with Coulomb Slater are equivalent to the more sophisticated ones. However, there is clear modulation in the results and the RVAP-PNP values are higher than the Coulomb Slater ones up to $N = 152$ but the tendency changes at that point and the differences are pretty large for larger neutron numbers where the fission barriers are low and t_{SF} small. This effect was not observed in Ref. [44] due to the choice of nuclei. We therefore conclude that the impact of Coulomb antipairing plus RVAP-PNP cannot be taken into account by the far more simple Coulomb Slater approximation. As already mentioned, the results discussed in this paper have been obtained with the Gogny-D1M* EDF. However, for the studied nuclei, calculations have also been carried out with other parametrizations, such as D1M [57] and D1S [4], of the Gogny-EDF. In all cases the results are similar to those obtained with the parameter set D1M*.

One has to take into account also that the intrinsic collective inertias have been used for the RVAP-PNP calculation. In principle, one could compute the exact GCM inertias with the PNP wave functions but unfortunately this is not the case for the ATDHFB approach. The inclusion of the "projected inertias" is out of the scope of the present study. Work along these lines is in progress and will be reported in future publications.

IV. SUMMARY AND CONCLUSIONS

In this work, we have considered a hierarchy of HFB based approximations as well as the RVAP-PNP method,
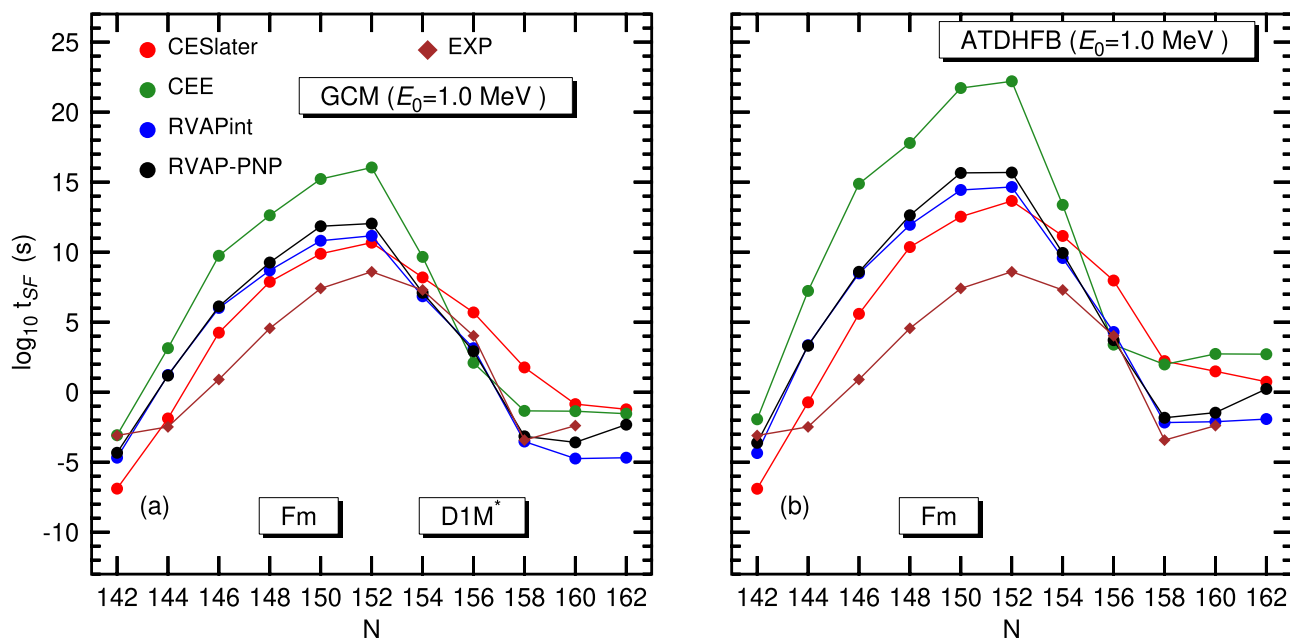
FIG. 7. The HFB(CESlater), HFB(CEE), HFB(RVAPint), and RVAP-PNP spontaneous fission half-lives, predicted within the GCM [panel (a)] and ATDHFB [panel (b)] schemes, for the isotopes $^{242-262}$Fm are depicted as functions of the neutron number. Calculations have been carried out with $E_0 = 1.0$ MeV. The available experimental values [53] are included in the plots. Results have been obtained with the parametrization D1M* of the Gogny-EDF.

based on the parametrization D1M* of the Gogny-EDF, to study the competition between Coulomb antipairing and dynamic pairing correlations along the fission paths of a selected set of Fermium and Nobelium isotopes. The considered isotopic chains include examples with wide fission paths as well as other cases where the fission paths exhibit a faster decline in their outer sections. The results obtained for the fission paths and other fission related quantities, such as
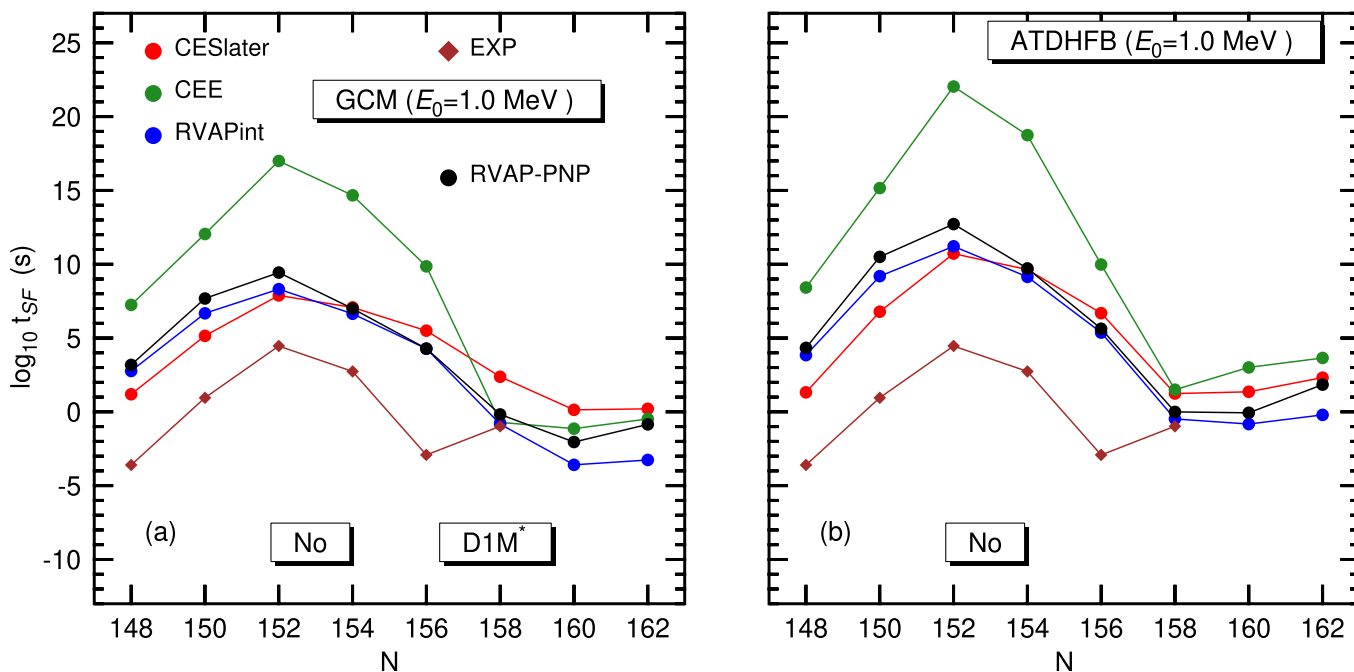
FIG. 8. The HFB(CESlater), HFB(CEE), HFB(RVAPint) and RVAP-PNP spontaneous fission half-lives, predicted within the GCM [panel (a)] and ATDHFB [panel (b)] schemes, for the isotopes $^{250-264}$No are depicted as functions of the neutron number. Calculations have been carried out with $E_0 = 1.0 MeV$. The available experimental values [53] are included in the plots. Results have been obtained with the parametrization D1M* of the Gogny-EDF.

the spontaneous fission half-lives t_{SF}, reveal that the impact of Coulomb antipairing (required to have a particle number restoration process free from self-energy problems) is partially compensated by dynamic pairing correlations induced via the RVAP-PNP procedure. The cancellation of both effects is, however, not perfect and a modulation of the t_{SF} values with respect to the plain mean-field is observed as a function of neutron number in the isotopic chains analyzed. Similar results have also been found with other parametrizations of the Gogny-EDF. The phenomenon is traced back

to the relatively low fission barriers found in some of the Fm and No isotopes. This situation is different from the one encountered in a previous analysis with the same techniques where nuclei with high barriers and wide fission paths were considered. We therefore conclude that the cancellation effect due to RVAP-PNP and Coulomb antipairing cannot be neglected in the most general situations. More general conclusions could be reached when the collective inertias would be computed in a consistent symmetry-restoration framework.

[1] N. Schunck and L. M. Robledo, Rep. Prog. Phys. **79**, 116301 (2016).

[2] P. Ring and P. Schuck, *The Nuclear Many-Body Problem* (Springer, Berlin, 1980).

[3] R. Rodríguez-Guzmán and L. M. Robledo, Phys. Rev. C **89**, 054310 (2014).

[4] J. F. Berger, M. Girod, and D. Gogny, Nucl. Phys. A **428**, 23 (1984).

[5] J.-P. Delaroche, M. Girod, H. Goutte, and J. Libert, Nucl. Phys. A **771**, 103 (2006).

[6] S. Perez-Martin and L. M. Robledo, Int. J. Mod. Phys. E **18**, 788 (2009).

[7] N. Dubray, H. Goutte, and J.-P. Delaroche, Phys. Rev. C **77**, 014310 (2008).

[8] V. Martin and L. M. Robledo, Int. J. Mod. Phys. E **18**, 861 (2009).

[9] W. Younes and D. Gogny, Phys. Rev. C **80**, 054313 (2009).

[10] M. Warda, J. L. Egido, L. M. Robledo, and K. Pomorski, Phys. Rev. C **66**, 014310 (2002).

[11] L. Egido and L. M. Robledo, Phys. Rev. Lett. **85**, 1198 (2000).

[12] M. Warda and J. L. Egido, Phys. Rev. C **86**, 014322 (2012).

[13] R. Rodríguez-Guzmán, Y. M. Humadi, and L. M. Robledo, Eur. Phys. J. A **56**, 43 (2020).

[14] N. Nikolov, N. Schunck, W. Nazarewicz, M. Bender, and J. Pei, Phys. Rev. C **83**, 034305 (2011).

[15] J. D. McDonnell, W. Nazarewicz, and J. A. Sheikh, Phys. Rev. C **87**, 054327 (2013).

[16] J. Erler, K. Langanke, H. P. Loens, G. Martínez-Pinedo, and P.-G. Reinhard, Phys. Rev. C **85**, 025802 (2012).

[17] A. Staszczak, A. Baran, and W. Nazarewicz, Phys. Rev. C **87**, 024320 (2013).

[18] A. Baran, K. Pomorski, A. Lukasiak, and A. Sobiczewski, Nucl. Phys. A **361**, 83 (1981).

[19] M. Baldo, L. M. Robledo, P. Schuck, and X. Viñas, Phys. Rev. C **87**, 064305 (2013).

[20] S. A. Giuliani and L. M. Robledo, Phys. Rev. C **88**, 054325 (2013).

[21] S. A. Giuliani, G. Martí nez-Pinedo, and L. M. Robledo, Phys. Rev. C **97**, 034323 (2018).

[22] H. Abusara, A. V. Afanasjev, and P. Ring, Phys. Rev. C **82**, 044303 (2010).

[23] H. Abusara, A. V. Afanasjev, and P. Ring, Phys. Rev. C **85**, 024314 (2012).

[24] B. N. Lu, E. G. Zhao, and S. G. Zhou, Phys. Rev. C **85**, 011301(R) (2012).

[25] S. Karatzikos, A. V. Afanasjev, G. A. Lalazissis, and P. Ring, Phys. Lett. B **689**, 72 (2010).

[26] M. Bender, K. Rutz, P.-G. Reinhard, J. A. Maruhn, and W. Greiner, Phys. Rev. C **58**, 2126 (1998).

[27] Z. Shi, A. V. Afanasjev, Z. P. Li, and J. Meng, Phys. Rev. C **99**, 064316 (2019).

[28] A. Taninah, S. E. Agbemava, and A. V. Afanasjev, Phys. Rev. C **102**, 054330 (2020).

[29] R. Rodríguez-Guzmán and L. M. Robledo, Eur. Phys. J. A **50**, 142 (2014).

[30] R. Rodríguez-Guzmán and L. M. Robledo, Eur. Phys. J. A **52**, 12 (2016).

[31] R. Rodríguez-Guzmán and L. M. Robledo, Eur. Phys. J. A **52**, 348 (2016).

[32] R. Rodríguez-Guzmán and L. M. Robledo, Eur. Phys. J. A **53**, 245 (2017).

[33] S. Pérez-Martín and L. M. Robledo, Phys. Rev. C **78**, 014304 (2008).

[34] J. Sadhukhan, K. Mazurek, A. Baran, J. Dobaczewski, W. Nazarewicz, and J. A. Sheikh, Phys. Rev. C **88**, 064314 (2013).

[35] S. A. Giuliani, L. M. Robledo, and R. Rodríguez-Guzmán, Phys. Rev. C **90**, 054311 (2014).

[36] M. Brack, J. Damgaard, A. S. Jensen, H. C. Pauli, V. M Strutinsky, and C. Y. Wong, Rev. Mod. Phys. **44**, 320 (1972).

[37] G. F. Bertsch and H. Flocard, Phys. Rev. C **43**, 2200 (1991).

[38] M. Urin and D. Zaretsky, Nucl. Phys. **75**, 101 (1966).

[39] K. Urin and D. Pomorski, Int. J. Mod. Phys. E **16**, 237 (2007).

[40] A. Staszczak, S. Pilat, and K. Pomorski, Nucl. Phys. A **504**, 589 (1989).

[41] J. Sadhukhan, W. Nazarewicz, and N. Schunck, Phys. Rev. C **93**, 011304(R) (2016).

[42] J. Zhao, B.-N. Lu, T. Niksic, D. Vretenar, and S.-G. Zhou, Phys. Rev. C **93**, 044315 (2016).

[43] R. Rodríguez-Guzmán and L. M. Robledo, Phys. Rev. C **98**, 034308 (2018).

[44] R. Bernard, S. A. Giuliani, and L. M. Robledo, Phys. Rev. C **99**, 064301 (2019).

[45] M. Bender, P.-H. Heenen, and P. Bonche, Phys. Rev. C **70**, 054304 (2004).

[46] M. Samyn, S. Goriely, and J. M. Pearson, Phys. Rev. C **72**, 044316 (2005).

[47] T. V. Nhan Hao, P. Quentin, and L. Bonneau, Phys. Rev. C **86**, 064307 (2012).

[48] P. Marević and Nicolas Schunck, Phys. Rev. Lett. **125**, 102504 (2020).

[49] M. Anguiano, J. L. Egido, and L. M. Robledo, Nucl. Phys. A **683**, 227 (2001).

[50] J. A. Sheikh, J. Dobaczewski, P. Ring, L. M. Robledo, and C. Yannouleas, J. Phys. G **48**, 123001 (2021).

[51] T. Lesinski, T. Duguet, K. Bennaceur, and J. Meyer, Eur. Phys. J. A **40**, 121 (2009).

[52] H. Nakada and M. Yamagami, Phys. Rev. C **83**, 031302(R) (2011).

[53] N. E. Holden and D. C. Hoffman, Pure Appl. Chem. **72**, 1525 (2000).

[54] T. R. Rodríguez, J. L. Egido, L. M. Robledo, and R. Rodríguez-Guzmán, Phys. Rev. C **71**, 044313 (2005).

[55] T. R. Rodríguez, J. L. Egido, and L. M. Robledo, Phys. Rev. C **72**, 064303 (2005).

[56] C. Gonzalez-Boquera, M. Centelles, X. Vinas, and L. M. Robledo, Phys. Lett. B **779**, 195 (2018).

[57] S. Goriely, S. Hilaire, M. Girod, and S. Péru, Phys. Rev. Lett. **102**, 242501 (2009).

[58] R. Rodríguez-Guzmán, L. M. Robledo, and P. Sarriguren, Phys. Rev. C **86**, 034336 (2012).

[59] L. M. Robledo and R. Rodríguez-Guzmán, J. Phys. G **39**, 105103 (2012).

[60] L. M. Robledo and G. F. Bertsch, Phys. Rev. C **84**, 014312 (2011).

[61] L. M. Robledo, Phys. Rev. C **79**, 021302(R) (2009).

[62] G. F. Bertsch and L. M. Robledo, Phys. Rev. Lett. **108**, 042505 (2012).

[63] C. Titin-Schnaider and Ph. Quentin, Phys. Lett. B **49**, 213 (1974).

[64] G. F. Bertsch, C. A. Bertulani, W. Nazarewicz, N. Schunck, and M. V. Stoitsov, Phys. Rev. C **79**, 034306 (2009).

[65] M. Girod and B. Grammaticos, Nucl. Phys. A **330**, 40 (1979).

[66] M. J. Giannoni and P. Quentin, Phys. Rev. C **21**, 2060 (1980); **21**, 2076 (1980).

[67] J. Libert, M. Girod, and J. P. Delaroche, Phys. Rev. C **60**, 054301 (1999).

[68] J. L. Egido and L. M. Robledo, Lect. Notes Phys. **641**, 269 (2004).

[69] R. R. Rodríguez-Guzmán, J. L. Egido, and L. M. Robledo, Phys. Lett. B **474**, 15 (2000); Phys. Rev. C **62**, 054308 (2000).

[70] R. Rodríguez-Guzmán, J. L. Egido, and L. M. Robledo, Nucl. Phys. A **709**, 201 (2002).

[71] J. Sadhukhan, J. Dobaczewski, W. Nazarewicz, J. A. Sheikh, and A. Baran, Phys. Rev. C **90**, 061304(R) (2014).